Case Studies in Thermal Engineering 74 (2025) 106991

Contents lists available at ScienceDirect

Case Studies in Thermal Engineering

journal homepage: www.elsevier.com/locate/csite

Innovative air duct-enhanced thermal management and natural convection heat transfer intensification in the busbar compartment of an air-insulated medium-voltage switchgear

Ondřej Novák [a,b], Lubomír Klimeš [b,*]

[a] ABB ELDS Brno, Vídeňská 100/117, 61900, Brno, Czech Republic
[b] Energy Institute, Brno University of Technology, Technická 2896/2, 61669, Brno, Czech Republic

GRAPHICAL ABSTRACT

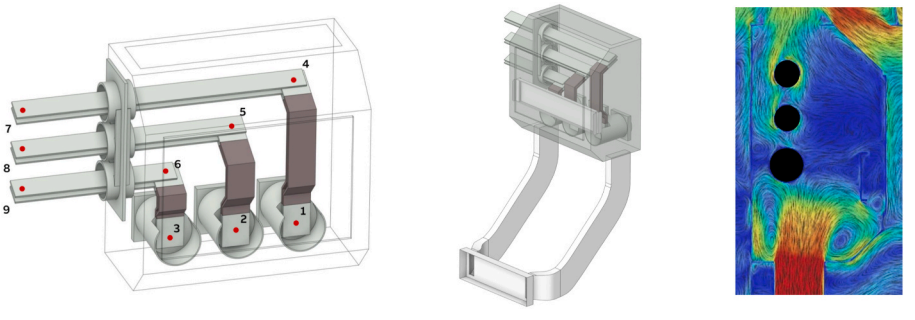

ABSTRACT

In the current development of medium-voltage switchgear systems, there is a strong demand for increasing electrical efficiency, performance, and reliability, necessitating effective thermal management. However, there is only limited knowledge about the thermal behaviour and possibilities for cooling intensification of air-insulated medium-voltage switchgears, frequently used in practice. The study presents an innovative way to enhance the cooling of a busbar compartment of an air-insulated medium voltage switchgear. This comprised a thermally efficient design of air ducts for enhanced convection. Several designs were proposed and investigated. The investigations involved multi-physical computer simulations, experimental investigations, and testing, including standardised temperature rise tests. Good agreement between simulations and experiments was achieved with an average root mean squared error of about 2.8 °C. Shape-optimisation of the proposed design with a two-channel ventilation duct system led to a 57 % decrease in the pressure drop of the ducts, reducing the relative temperature rise in the busbar compartment by about 10 %–

* Corresponding author.
E-mail address: klimes@fme.vutbr.cz (L. Klimeš).

https://doi.org/10.1016/j.csite.2025.106991

Available online 5 September 2025

25 % compared to other investigated designs. Such a superiority was also confirmed in experimental investigations in a certified laboratory. This makes the proposed design very promising for enhanced cooling and easy adaptation of the switchgear for various applications, including the increase in its current rating.

1. Introduction

Medium-voltage air-insulated switchgears are significant parts of the electrical grid, and their production represents an important and economically attractive market [1]. An increasing electricity demand has resulted in a need to raise the current ratings of switchgear. However, according to Joule's law, higher electrical currents lead to more significant power loss. As the current ratings increase, medium-voltage switchgears reach their thermal limits defined by the IEC standard 62271–200 [2]. Faults caused by overheating busbar conductors are a common source of accidents, as reported, e.g. by Runde [3]. This issue demands economical solutions for reducing the temperature rise in current-carrying paths while maintaining reliability and safety, which are crucial for the stability of power systems [4].

A medium-voltage air-insulated switchgear is typically divided into several compartments, one separated from the other by thick metal sheets [5]. The structure of the switchgear and the arrangement of compartments depend on standards applicable to a target market (e.g. the standard series IEC 62271) and also on the requirements of the customer. The design must prevent pressure waves and hot gases due to internal arcs, which could cause injury to workers near the switchgear. It also protects other components from internal arc damage, which could disrupt the operation of the switchgear. The busbar compartment, usually enclosed by other compartments, suffers from restricted airflow intake necessary for cooling. Another typical case is when hot air from adjacent compartments enters the busbar compartment. As a result, overheating in the busbar compartment significantly limits the maximum current rating of the medium-voltage switchgear.

Besides considerations related to the thermal management of switchgear, economic factors must also be considered in the design. A critical issue, which affects the economic viability and competitiveness, is related to the consumption of copper in the switchgear. Increasing the cross-sectional area of copper conductors is a simple way to reduce power loss, mitigating the need for thermal management of the switchgear. However, the cost of copper conductors in the busbar compartment of the switchgear accounts for about 50 % of the total costs [6], which means that the consumption of copper is strictly optimised for economic reasons. The improvement of thermal management of the switchgear is, therefore, directly related to the amount of copper used in the switchgear. Simply speaking, the better the thermal management and cooling of compartments without increasing cross-sections of conductors, the lower the amount of copper needed to keep the current rating of the switchgear unchanged.

As for the thermal assessment and analysis of switchgears, empirical formulas and a thermal network method were frequently used to determine the power loss and the temperature rise in the switchgear compartments. Though these approaches were extensively utilised in the past, their use is nowadays somewhat limited as they rely on data from existing prototypes, restricting their ability to assess advanced designs and new ideas [7]. Significant advancements in computer performance in the last two decades have given rise to powerful simulation tools for addressing multi-physical problems, including the thermal analysis of electrical switchgears. Ho et al. [8] created a 3D eddy-current model of solid-insulated busbars. Even though the model oversimplified convective and radiative heat transfer, the presented results had a straightforward application potential. However, the applicability of the results is limited as the study did not focus on air-insulated systems. Anbo et al. [9] presented a one-way coupling of an eddy-current and CFD-based thermal model for an air-insulated busbar trunking system. Simulations included flow fields and eddy-current effects, and the results indicated improved simulation accuracy. However, the geometry considered in modelling was only a 2D cross-section, bringing a significant simplification when compared to an actual switchgear. Wang et al. [10] conducted a thermal analysis of an isolated phase bus system. The study and presented results emphasised the importance of the analysis of velocity vector fields for improving switchgear performance. Anyway, similarly to the study presented by Anbo et al. [9], the geometry considered in the study was substantially simplified, which limits its practical implications.

Paulke et al. [11] simulated thermal effects related to arc switching, which is also partially relevant to complete switchgear systems. Their study assumed steady-state conditions for heat transfer, but some significant simplifications were adopted in the analysis. The study accounted for power losses due to the electrical contact resistance, which is an essential factor in the thermal analysis of switchgear. Kim et al. [12,13] proposed a method for predicting the temperature rise in the switchgear based on the determination of power loss through an electromagnetic analysis. The main focus was on estimating power loss in extra-high-voltage busbars. The estimation was used afterwards as a heat source in simulations. The results obtained with the proposed method were compared to experimental data. Even though an improvement in the prediction was observed when compared to other methods assuming a constant heat transfer coefficient, the accuracy of the prediction was still unsatisfactory. Since the quantification of convective heat transfer appeared complex and challenging in previous studies, Guan et al. [14] applied a lattice Boltzmann method to simulate heat transfer processes inside gas-insulated switchgear capsules. The lattice Boltzmann method benefits from lower hardware requirements when compared to conventional CFD simulations using Reynolds-average Navier-Stokes (RANS) models. Even though the technique oversimplified the power loss due to using equivalent heat flux, the results demonstrated that the approach is quite a simple and efficient tool for thermal simulations with desirable accuracy.

In a study presented by Wang et al. [15], a 252 kV gas-insulated busbar chamber was investigated. The geometry of busbars included pipes fitted in a three-phase tubular design. Besides the temperature rise, the study also addressed insulating gas breakdown. In the studied case, skin effects yielded a 12.2 % increase in power loss generation. The proximity effect was neglected, even though the

distance between phases was smaller than in the present study. Further, the authors investigated the temperature dependency of the electric conductivity, and they reported a 13.2 % change in its value. This conclusion confirms the findings reported by Bedkowski et al. [16], who pointed out that two-way coupling is necessary. Research on condensation in medium-voltage switchgear was reported by Zheng et al. [17]. The study proved that a detailed thermal analysis of a medium-voltage switchgear can be done using CFD with a conventional RANS model. Air-conditioning-based dehumidification was proposed to prevent condensation of the switchgear. In the study, the authors addressed several designs of air-conditioning jets, including flow visualisation. The results demonstrated that the dehumidification of the proposed system is satisfactory, as the surface temperature of the switchgear can be up to almost 8 °C higher than the dew point of the returning air. In another study, Shu et al. [18] also studied condensation in a high-voltage switchgear, which was, to a certain extent, similar to that in the study by Zheng et al. [17]. The study focused on the prediction of condensation using CFD simulations and their accuracy. The authors concluded that simulation results agreed with experimental data as the relative error was up to ±6 %.

Bedkowski et al. [16] proposed a computational methodology for coupling thermal and electrical simulations, considering a balance between the precision and computational cost. The authors reported a relative error of 5.9 % and found that two-way coupling was necessary for accurate results. Such a conclusion was confirmed with data from the experimental temperature rise test (TRT), and such data were used for validation. In their follow-up study, Bedkowski et al. [19] presented optimisation of the cooling performance of low-voltage switchgear using multi-physical simulations. The study focused solely on the evaluation of temperature rise at predefined positions. Such an approach is prevalent in industry when data from TRTs are analysed. However, the authors failed to address airflow parameters and flow structures, and no in-depth analysis and optimisation based on post-processing of results was presented. In another study, using a genetic algorithm, Bedkowski et al. [6] applied 2.5D multi-layer optimisation to minimise surface area and power loss in the busbar compartment. Although this approach led to reduced use of copper in the cross-section area, it also caused an increase in power loss and temperature rise, limiting its applicability.

Matin et al. [20] developed an artificial intelligence-based predictive model of the temperature rise in a medium voltage switchgear. CFD simulations were used to obtain learning data, and predicted values with the R-squared value above 90 % indicated a good quality of the prediction. However, only 67 variants of the switchgear operation were simulated with considerable simplifications, which limits the direct use of the model in industrial applications. Aguirre et al. [21] analysed the temperature rise of a single conductor joint. However, only a finite element method (FEM)-based model, which was rather simple compared to other studies, e.g. by Bedkowski [6,16,19], was utilised. Furthermore, the electrical contact resistance was not evaluated, and only the resistance for the complete configuration setup was presented, which limits the use of the results. On the other hand, a relevant uncertainty analysis employing Monte Carlo methods was presented, justifying the adopted methodology.

A very relevant study was presented by Zheng et al. [22], who performed a thermal study of a medium voltage switchgear. Although it was not claimed in the study, a commercially produced and sold industrial switchgear design with vertical busbars typical for certain markets was very likely investigated. The study addressed several locations of air intakes for natural convection, and the influence of forced convection was also analysed and compared. Even though the computational mesh was quite coarse and a rather overestimated value of the electrical conductivity (almost 6 MS/m) was considered, a good agreement between the simulated and experimental data was achieved. Flow separations and recirculation regions visible in the results could be further reduced by shape optimisation. The results also indicated that the value of the heat transfer coefficient was not higher than 4 $W/(m^2K)$. Cheng et al. [23] proposed and validated a novel computational approach, in which each layer around a circular conductor was modelled as a resistance. The total resistance was then determined as a sum of individual layer-based resistances, as in the case of electrical resistors. The proposed technique was validated and compared to CFD. Considering the simplicity of the suggested approach, the results correlated quite well with data obtained from CFD simulations. Even though such a simplified method works well only for configurations where the cross-section of the conductor (current path) remains nearly constant, the proposed method can be well applicable, e.g. for initial sizing of a switchgear.

An interesting solution for thermal management was proposed by Qu et al. [24] who investigated heat withdrawal from an electronic cabinet by means of a fined radiator and embedded heat pipes. The study mainly addressed a forced convection design, but the proposed solution seems to be also easily transferable to a natural convection-based design. The heat pipes can be replaced by (cheaper) metallic rods, and fin size and spacing and size can be adapted to natural convection cooling. An issue can be a dielectric discharge during an impulse level test, but this could be solved by hiding the heat sink within the electric field of conductors, as already proposed by Kaufmann et al. [25]. In a related study reported by Yu et al. [26], the authors investigated a medium-voltage switchgear with several modifications of a heat exchanger with heat pipes. Their results demonstrated that shortening the current path and changing the position of the transformer had a positive effect on the temperature rise. Although the proposed solution enhanced thermal performance, economic considerations crucial for the real-life application were not evaluated.

Several solutions have been proposed to tackle the above-mentioned issues leading to overheating. One obvious solution is to utilise forced convection cooling, e.g. using fans as suggested by Kaufmann et al. [27]. However, a substantial drawback of fans is their limited lifespan and proneness to malfunction, which implies a need for additional maintenance, reduced reliability, and extra costs. Another option is the use of heat pipes. Previously used heat pipes employed sulfur hexafluoride (SF_6) as a medium due to its good thermal and electrical insulating properties. However, gases like SF_6 are being phased out due to their environmental impact [28]. Heat pipes were considered expensive and unreliable for air-insulated medium-voltage switchgear even before the SF_6 ban in Europe. Now, even more complicated solutions have to be devised as proposed. For example, the solution proposed by Kessler et al. [29] is SF_6-free but not free of per- and polyfluoroalkyl substances (PFAS). Another solution proposed in the study by Kessler et al. avoided using SF_6 and PFAS but utilised a very expensive electrically insulating ceramic sub-component [30]. Even though heat pipes are commonly used in gas-insulated switchgears, they are rather costly, and their use also leads to an increased risk of failure, regardless of

the gas used. Neither forced convection cooling nor heat pipes represents a solution that would meet the technical and economic requirements of the producers of air-insulated medium-voltage switchgears. In this respect, Los [31] computationally addressed passive cooling of the busbar compartment of a medium-voltage switchgear and presented a detailed cost-effectiveness analysis of the proposed solutions. He concluded that from the viewpoint of cost efficiency, the optimisation of radiative heat transfer is the best option. On the other hand, the shape optimisation of the primary cooling component was identified as the worst solution.

Another solution to thermal management of various systems, already well researched in relation to e.g. photovoltaic systems [32] and battery energy storage systems [33], is the utilisation of phase change materials (PCMs). A PCM is a material which is able to change its phase (e.g. from liquid to solid and vice versa) in a specific and relatively narrow temperature range. These phase transitions are associated with the release and accumulation of heat. Such heat is referred to as latent heat, meaning that, in contrast to the sensible heat, the latent heat (nearly) does not change the temperature of the matter. A PCM properly selected for a certain application can therefore act as a heat sink or a heat source, enabling it to stabilise (maintain) the temperature of the system and/or to prevent its overheating or undercooling. However, the knowledge about the utilisation of PCMs in electrical switchgears is very limited in the current literature.

As can be concluded from the presented overview of the published papers and their comparison presented in Table 1, some research studies have been published on thermal management in low-voltage switchgears and gas-insulated medium-voltage switchgears, extensively adopting multi-physical simulations in investigations. As for medium-voltage air-insulated switchgears, only a limited number of studies were reported, mainly focusing on condensation issues. None of the published papers addressed, in detail, the thermal management and heat withdrawal intensification in medium-voltage air-insulated switchgear, employing both technically and economically efficient approaches with natural convection cooling. There is also a lack of studies which would address the optimisation of air/gas flow inside the switchgear, particularly from the aerodynamic viewpoint. Another important limitation and issue associated with the published papers is the insufficient validation of computational results. As listed in Table 1, most of the studies involved the temperature rise test, but only for a simplified (mockup) design or using non-original data, while full-scale experiments are scarce. The present paper aims to fill this research gap and proposes a novel solution to thermal management in a medium-voltage air-insulated switchgear, employing specifically designed ducts to feed ambient air into the busbar compartment for natural convection cooling. The switchgear for a current rating of 4000 A and a current frequency of 50 Hz was considered in the study. Comprehensive investigations, including various designs of ducts, outlets, and insulation configurations, were carried out using coupled CFD-electromagnetic simulations and full-scale experimental testing, including TRTs and anemometric measurements.

2. Experimental setup

In practice, switchgears produced and available for commercial use must comply with various standards, including the standard series IEC 62271. A part of the series, the standard IEC 62271–200 applies to prefabricated alternating current metal-enclosed switchgears for the range of the rated voltage between 1 kV (excluded) and 52 kV (included), both air-insulated and fluid-insulated versions for indoor as well as outdoor installation. The standard also defines a methodology for switchgear testing, including the TRT. Since the standard IEC 62271–200 applies to the switchgear investigated in the present study, the experimental investigations were done following that standard in a certified laboratory affiliated with the ABB company in Brno, in the Czech Republic. The experimental part involved TRTs; the acquired data were used to validate simulation models. The experimental data were also used to assess the optimised design of the switchgear.

The certified accuracy in the TRT was ±1 % of the measured thermodynamic temperature (in Kelvin). Wire thermocouples (type L) with a resolution of 0.1 K were used for the temperature measurement in the TRT. The thermocouples were connected to a digital thermometer, part of a multi-channel temperature measurement system. The measurement system was specifically designed, manufactured, and certified at the Central European Institute of Technology (CEITEC) in Brno, Czech Republic. The thermocouples used for the temperature measurement in the solid parts of the switchgear were placed in holes drilled into the components. Besides the temperature measurement in solid parts, the air temperature inside the switchgear at various positions was also measured. The TRT involved the temperature measurement of solid parts and air at about 100 positions on all three phases along the current path. Fig. 1 shows the current path in the busbar compartment with locations of nine thermocouples, including three thermocouples for connections to upper pin contact of each phase L1, L2, and L3 (positions 1–3 in Fig. 1), three thermocouples for connections of T-off with the busbar of each phase L1, L2, and L3 (positions 4–6 in Fig. 1), and three thermocouples for the end of the busbar of each phase L1, L2, and L3 (positions 7–9 in Fig. 1).

A schematic of the TRT is shown in Fig. 2. A switchgear assembly was positioned in a laboratory, a sufficiently large room providing a considerable distance between the switchgear assembly and the room walls. Electric cables from a transformer, conducting the electric current, were connected to the switchgear from its bottom. The electric current conduction ended in a neutral point, which was covered by a thermally insulating layer. The ambient temperature was measured using a thermocouple in a container filled with oil. The oil, in which the temperature sensor was immersed, was used to stabilise the temperature measurement and to prevent the measurement from fluctuations and inaccuracy due to the movement and turbulence of the surrounding air inside the laboratory.

The TRT was performed with the switchgear loaded by an alternating three-phase current of 4000 A and a frequency of 50 Hz. The voltage during the TRT was kept very low, which did not influence the TRT results. The switchgear was connected to a large transformer with cables leading to the cable compartment from the bottom of the switchgear. As indicated in Fig. 2, the short-circuiting device did not earth the circuit, meaning the circuit breaker did not interrupt the circuit. The circuit ended outside of the switchgear at a neutral point. In each TRT, only a single panel configuration was tested. However, several panels positioned next to one another are used in practice. To consider such a configuration, the standard IEC 62271–200 requires a polystyrene wall with a

Table 1
Overview of research works related to the investigation of electrical switchgears (ordered from newest to oldest).

Reference	Year	Modelling approach	Investigated system	Convection heat transfer	Design proposal or modification	Validation
Matin et al. [20]	2025	EMAG + CFD, one-/two-way coupling not specified	Medium-voltage air-insulated switchgear	Forced convection	None	None
Aguirre et al. [21]	2025	ElmerFEM, Monte Carlo	Busbar bolted joint	Not specified	None	Temperature rise for a mockup design
Yu et al. [26]	2025	EMAG + CFD, one-/two-way coupling not specified	Medium-voltage air-insulated switchgear	Natural and forced convection	Heat exchanger design	Non-original data
Cheng et al. [23]	2024	A thermal network method, CFD	Gas-insulated transmission lines	Natural convection	Parametric dimension of the device	Non-original data
Zheng et al. [22]	2023	EMAG + CFD, one-/two-way coupling not specified	Medium-voltage air-insulated switchgear	Natural and forced convection	Location of openings	Temperature rise for a mockup design
Shu et al. [18]	2023	CFD + condensation	Medium-voltage air-insulated switchgear	Natural convection	None	Temperature rise for a mockup design
Qu et al. [24]	2022	CFD, a thermal resistance model	Finned radiator with a heat pipe	Natural and forced convection	Design of a finned radiator with a heat pipe	Temperature rise for a mockup design
Wang et al. [15]	2022	EMAG + CFD, two-way coupling	High-voltage gas-insulated switchgear	Natural convection	None	Temperature rise for a mockup design
Guan et al. [14]	2021	Lattice-Boltzmann method	Gas-insulated capsule for unspecified voltage level	Natural convection	None	Temperature rise for a mockup design
Zheng et al. [17]	2021	CFD + condensation	Medium-voltage air-insulated switchgear	Natural and forced convection	Supply air duct for moisture control	Humidity distribution
Bedkowski et al. [19]	2017	EMAG + CFD, two-way coupling	Low-voltage air-insulated switchgear	Natural convection	None	Temperature rise for a mockup design
Bedkowski et al. [6]	2016	EMAG + CFD, two-way coupling	Low-voltage air-insulated switchgear	Natural convection	Optimised cross-sections of busbars	Non-original data
Bedkowski et al. [34]	2016	EMAG + CFD, two-way coupling	Low-voltage air-insulated switchgear	Natural convection	None	Temperature rise for a mockup design
Stosur et al. [7]	2016	Thermal network model	Medium-voltage gas-insulated switchgear	Natural convection	None	Temperature rise for a mockup design
Bedkowski et al. [16]	2014	EMAG + CFD, two-way coupling	Low-voltage air-insulated switchgear	Natural convection	None	Temperature rise
Gastelurrutia et al. [35]	2011	CFD	Distribution transformers	Natural convection (in oil)	None	Temperature rise for a mockup design
Wang et al. [10]	2007	EMAG + CFD, one-/two-way coupling not specified	Isolated–phase bus	Forced convection	Inlet positions	Temperature rise for a mockup design
Kim et al. [13]	2005	EMAG FEM + heat transfer coefficient specification	Extra-high-voltage gas-insulated switchgear busbar	Natural convection	None	Temperature rise for a mockup design
Sigey et al. [36]	2004	Numerical solution of governing PDEs via Samarskii–Andreyev ADI scheme	Enclosure	Natural convection	None	Temperature rise for a mockup design
Ho et al. [8]	2003	EMAG + solution of thermal PDEs	Isolated phase bus	Natural convection	None	Temperature rise for a mockup design
Behzadmehr et al. [37]	2003	Experimental investigation	Vertical tubes	Mixed convection	None	Lab-scale experiments
Anbo et al. [9]	2002	EMAG + CFD, one-/two-way coupling not specified	Busbar trunking systems	Natural convection	Size recommendation for shielding	Temperature rise for a mockup design
Kim et al. [12]	2002	Coupled FEM-analytic technique	Extra-high-voltage busbar	Natural convection	None	Non-original data
Paulke et al. [11]	2001	CFD	Arc switching	Arc heat generation	None	Temperature rise for a mockup design

(*continued on next page*)

Table 1 (*continued*)

Reference	Year	Modelling approach	Investigated system	Convection heat transfer	Design proposal or modification	Validation
Fedorov and Viskanta [38]	1997	Experimental investigation	Vertical parallel plate channel	Natural convection	None	Lab-scale channel experiments
Shao et al. [39]	1995	CFD	HVAC duct fittings	Forced convection	Duct design	Lab-scale duct experiments
Hus [40]	1989	Dedicated method	Direct current busbars	Natural convection and liquid cooling	None	Non-original data

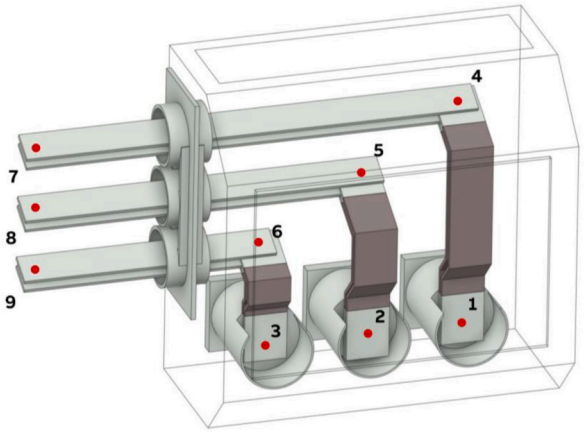

Fig. 1. Current path in the busbar compartment with positions of temperature measurements. Positions 1, 2, 3: Connection to the upper pin contact of phases L1, L2, and L3, respectively. Positions 4, 5, 6: Connection of T-offs and bus-bars of phases L1, L2, and L3, respectively. Positions 7, 8, 9: End of the busbar of phases L1, L2, and L3, respectively.

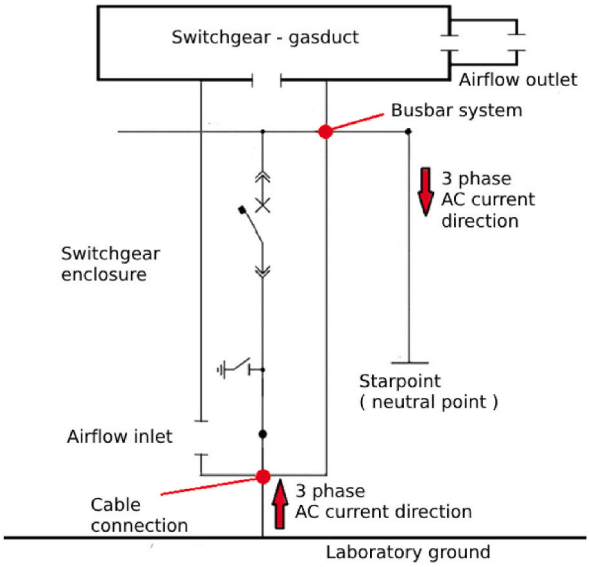

Fig. 2. A schematic of the TRT [41].

thickness of 50 mm to be installed on the side walls of the switchgear. The TRTs usually lasted several hours. The condition for terminating the test was that the temperature rise in all the measured positions must not exceed 1 K during the last 60 min.

3. Computer simulations

A thermal management simulation in the considered medium-voltage air-insulated switchgear necessitates the consideration of several phenomena, including heat transfer, fluid flow, and electromagnetism. Due to this reason, a coupling of two simulation tools was adopted to build a realistic simulation model. Heat transfer and fluid flow phenomena were solved using ANSYS Fluent software. The electromagnetic part of the problem, including the determination of the current density distribution and the power loss, was addressed in ANSYS Maxwell software. These two simulation tools were coupled since electromagnetic phenomena influence the thermal behaviour of the system, and, on the contrary, changes in the temperature influence the electrical conductivity of materials in electromagnetic simulation. Due to this reason, a two-way coupled problem was solved. The main factors of the adopted simulation model are presented in detail in the following sections.

3.1. Heat transfer and fluid flow

The thermal part of the model aimed at a solution of conjugate heat transfer (coupled heat transfer and fluid flow) in the switchgear, including its solid parts and the air inside and outside the switchgear. Radiative heat transfer was also taken into account, as detailed below. Therefore, the simulation model determined the temperature distribution in solids, air, and air velocity and pressure from the fundamental governing equations for energy, continuity, and momentum [42]. Since air velocities in the studied problem were much smaller than the speed of sound, the air was considered an incompressible fluid. This assumption is also taken into consideration in the following governing equations. The energy equation for both solids and fluids reads

$$\varrho\left(c_p\frac{\partial T}{\partial t}+u\cdot\nabla T\right)=\nabla\cdot(k\nabla T)+\dot{Q}_s \tag{1}$$

where T is the temperature, u denotes the velocity, t is time, ϱ is the density, c_p is the heat capacity at constant pressure, and k stands for the thermal conductivity. The last term $\dot{Q}_s$ in Eq. (1) is an internal volumetric heat source, accounting for power losses in electric current paths. These power losses are caused by Joule heating, the proximity effect, and the skin effect [43].

The solution of fluid dynamics (airflow in the switchgear) further involved the continuity equation

$$\frac{\partial\varrho}{\partial t}+\nabla\cdot(\varrho u)=0 \tag{2}$$

and the momentum equation, resulting in the Navier-Stokes equation

$$\varrho\left(\frac{\partial u}{\partial t}+u\cdot\nabla u\right)=\mu\nabla^2 u-\nabla p+(\varrho-\varrho_0)g \tag{3}$$

where p is the pressure, μ is the dynamic viscosity of the fluid, and g is the gravitational acceleration. The Reynolds-averaged Navier-Stokes (RANS) approach was adopted in the simulation model.

Besides heat conduction and convection, the simulation model also addressed radiative heat transfer for high accuracy of simulated results. A discrete ordinate (DO) model was adopted for this purpose. The DO model was used to solve both internal and external radiation. Internal radiation refers to thermal radiation among surfaces inside the enclosure of the switchgear. In contrast, external radiation involves thermal radiation between the outer surfaces of the switchgear and the ambient environment. Compared to a surface-to-surface radiation model, another approach for the computational solution of radiative heat transfer, the DO model benefits from better computational efficiency and straightforward use.

3.2. Electromagnetics

The electromagnetic part of the model was used to determine the distribution and density of electric current in electrically conductive parts and electric paths of the switchgear. This procedure allowed the identification of power losses and their distribution, which is directly related to the heat generation in Eq. (1). The electromagnetic simulation necessitated a solution of Maxwell's equations [44], which is a set of coupled equations describing the behaviour of electric and magnetic fields. These equations include Gauss's law

$$\nabla\cdot E=\frac{\varrho_e}{\varepsilon_0} \tag{4}$$

where E is the electric field, ϱ_e is the density of electric charge, and ε_0 is the vacuum permittivity; Gauss's law for magnetism

$$\nabla\cdot B=0 \tag{5}$$

stating that the magnetic field B complies with a solenoidal vector field; Faraday's law in the form of the Maxwell-Faraday equation

$$\nabla \times \mathrm{E} = -\frac{\partial \mathrm{B}}{\partial \mathrm{t}} \tag{6}$$

relating the electric and magnetic fields to each other and stating that a variation of the magnetic field in time coincides with a curl of the electric field, and the Ampère-Maxwell law

$$\nabla \times \mathrm{B} = \mu_0 \left(\mathrm{J} + \varepsilon_0 \frac{\partial \mathrm{E}}{\partial \mathrm{t}} \right) \tag{7}$$

where J is the current density and μ_0 is the vacuum permeability, claiming that the magnetic field is associated with the electric current and variations of the electric field in time. The power loss (dissipation) can be eventually determined from the solution of Maxwell's equations [45] as

$$\mathrm{P}_{\mathrm{loss}} = \sigma \int_{\mathrm{V}} |\mathrm{E}|^2 \, \mathrm{dV} \tag{8}$$

where σ is the electrical conductivity. The power loss determined according to Eq. (8) was substituted into the energy conservation law in Eq. (1) via the internal volumetric heat source $\dot{\mathrm{Q}}_{\mathrm{s}}$.

3.3. Turbulence modelling

Turbulence is a phenomenon that can significantly influence fluid flow dynamics and temperature distribution. Bedkowski et al. [16] reported on computer modelling of power loss generation in low-voltage switchgear, and they pointed out a relatively high turbulence intensity for air flowing through the switchgear. Based on their previous results for natural convection problems, including significant heat generation, they adopted a modified k-ε turbulence model. The authors in Ref. [16] also claimed that the k-ε turbulence model was successfully applied in a previous solution of airflow in longitudinal, horizontal and vertical ducts [38,39], buoyancy-driven flows in ducts [37] and enclosures [36], which is also the case investigated in the present paper. In a follow-up study, Bedkowski et al. [19] investigated cooling enhancement in an industrial low-voltage switchgear using a coupled simulation model employing a renormalisation group (RNG) k-ε turbulence model. The authors reported the Rayleigh number (Ra) for assessing the natural convection of $3 \cdot 10^9$, indicating the turbulent flow, which is assumed for the Ra number greater than $3 \cdot 10^5$. An identical methodology was adopted, directly comparing results and conclusions in Ref. [19]. The Ra number for the medium-voltage switchgear investigated in the present paper was $2.4 \cdot 10^8$ in the busbar compartment, indicating that the behaviour related to turbulence and natural convection should be similar to that in Ref. [19].

Motivated by the results and conclusions presented in the foregoing paragraph, a realisable **k-ε** turbulence model with an enhanced treatment of wall functions was used in the present study. Laminar and Menter's shear stress transport (SST) turbulence models were also tested. Using a laminar model led to unrealistic (too high) temperature rise values compared to experimental data. This observation indicated that turbulence is a key phenomenon for intensifying heat transfer withdrawal from the switchgear. In the case of the realisable **k-ε** and SST turbulence models, both models led to similar fluid temperatures, which agreed with experimental data. However, when velocity and wake profiles were considered, good agreement with experimental data was observed for the realisable **k-ε** model, while some discrepancies were present in the case of the SST model. The use of the realisable **k-ε** model was also supported by its reliability for industrial applications, as emphasised, e.g. by Gastelurrutia et al. [35], who numerically investigated natural

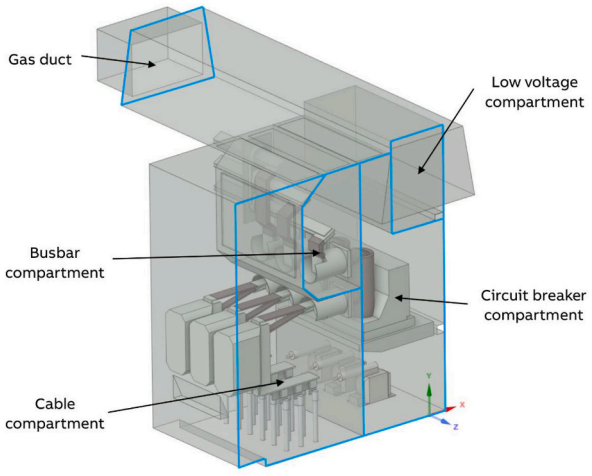

Fig. 3. Schematic of the medium-voltage switchgear and its main compartments.

convection in electrical transformers. Transport equations and other details of the realisable **k-ε** turbulence model are not presented here, as can be found elsewhere, e.g. in Ref. [19].

3.4. Geometry and simulation domain

The medium-voltage switchgear investigated in this study was an actual switchgear for industrial use. The switchgear contained a main current path with three-phase conductors, having a 275 mm insulation distance between the phases and other conductive components. The overall dimensions of the switchgear (its enclosure) were as follows: width of 1000 mm, height of 2850 mm, and depth of 1900 mm. The switchgear was divided into several compartments: a cable compartment, a circuit breaker compartment, a busbar compartment, a low-voltage compartment, and a gas duct.

The current path in the busbar compartment was covered by a steel enclosure, as indicated in Fig. 3. The vertical busbars consisted of 3 bars. Three conductors in each of the horizontal busbars had a more complex cross-section geometry with a similar cross-section area compared to the vertical busbars. A small gap separated the conductors from each other. The particular cross-section geometry of the conductors is not presented here due to confidentiality reasons. Bolted joints between the horizontal and vertical busbars were enclosed in plastic dielectric covers.

The switchgear was fitted with a circuit breaker, which allowed protective interruption of the current flow in case of overload or short circuit. The circuit breaker was made from three vacuum-interrupting embedded poles, each enclosed in an epoxy shell. The cable and circuit breaker compartments had inlet ventilation flaps, each fitted with a protective grid. The circuit breaker compartment was equipped with an IP4X grade grid at the inlet, while the cable compartment was fitted with an IP2X grade grid. The busbar compartment contained no air intakes from the ambient, even though its prototype was initially equipped with internal arc flaps of an IP2X grade. The busbar, cable, and circuit breaker compartments had an opening on their tops with IP2X grade protection. These openings were connected to the gas duct located above, which provided ventilation through an IP2X grade grid.

Two separate geometries (variants) of the computational domain were used in the simulation model of the switchgear, one for the thermal part and another for the electromagnetic part of the model, fulfilling the requirements of the solvers. The electromagnetic solver ANSYS Maxwell required a geometry with only components under high voltage. As a result, all components of the current path, which were made of copper and aluminium, were included in the geometry for the electromagnetic solver. Aluminium heat sinks were also included in the geometry, even though their contribution to the total power loss can be considered negligible. Similarly, metal sheet components also, to a small extent, contribute to the generated power loss, but these components were omitted to reduce the computational cost. For the same reason, the geometry for electromagnetic simulation had all fillets and holes for bolt connections removed, which had a very minor influence on the results. In the case of body-to-body contacts, a resistive sheet function was applied to simulate the electrical contact resistance. The geometry for the conjugate heat transfer solver consisted of 2D and 3D elements. The 2D elements were used for metal components and insulating sleeves of conductors. In contrast, the 3D elements were used for the current path, heat sinks, insulators, epoxy chambers, and other plastic and epoxy components with intricate geometry. Air ducts were modelled using 2D walls with the corresponding thickness and material properties. Heat conduction in the walls of air ducts was considered only in the direction perpendicular to the surface of duct walls, while other directions were neglected for their very minor effects.

3.5. Computational mesh

The mesh generation for electromagnetic simulations employed an adaptive discretisation algorithm [46], which was based on an iterative procedure, increasing the number of mesh elements until the energy imbalance becomes negligible with both the discrepancy in energy of the magnetic field and with the converged total power loss. The computational mesh for the electromagnetic solver consisted of tetrahedral elements. On the other hand, the mesh for conjugate heat transfer was prepared in advance using polyhedral elements. Seven layers of prismatic cells with a uniform height were used in the vicinity of surfaces to capture large thermal and

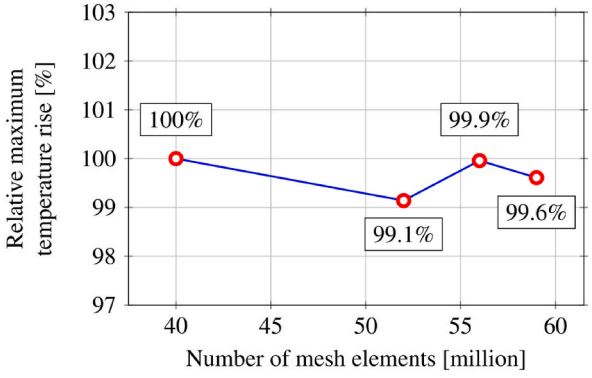

Fig. 4. Mesh dependency study and influence of the number of mesh elements on the relative maximum temperature rise.

momentum gradients in boundary layers.

The setup and configuration of the computational mesh involved a mesh dependency study, the results of which are presented in Fig. 4. The minimal number of mesh elements for which the simulation was completed was 40 million. As shown in Fig. 4, increasing the number of mesh elements brought only very minor changes in the relative maximum temperature rise, although the stability of simulations was gradually significantly improved. Due to this reason, the results presented in this study were obtained for the mesh with 56 million elements. The investigation revealed that the most critical mesh parts for thermal simulations are near-wall regions with thermal and momentum boundary layers. Following the recommendation in Ref. [46], the target y-plus value was one and well below five on all the surfaces. Special attention was paid to ensuring that both types of boundary layers were inside the layer of prismatic cells. The mesh density was significantly increased on all the solid surfaces and further refined on important faces, including domain interfaces and ventilation inlets and outlets. The computational mesh for conjugate heat transfer simulations was fully conformal. The mesh quality was assessed by means of the orthogonal mesh quality measure. The value of the orthogonal quality was above 0.15 in all cases.

Fig. 5 shows the influence of the number of mesh elements on the temperature rise along a path above the L1 conductor in the busbar compartment. As can be seen, there is only a minor discrepancy up to about 1 °C when results obtained with the use of different meshes are compared to each other. Similar conclusions can also be drawn for the air velocities (discrepancies up to about 0.03 m/s), which are presented in Fig. 6.

3.6. Coupling of electromagnetics with conjugate heat transfer

As explained above, two-way thermal-electromagnetic coupling was deployed to achieve high accuracy. The coupled simulation started with an initial solution of the electromagnetic part, assuming a constant temperature distribution of 100 °C within the entire computational domain. Once the initial electromagnetic simulation was completed, the power loss distribution was transferred to the thermal solver for the conjugate heat transfer simulation. The thermal solver performed 500 iterations, completing the initial simulation. Consequently, the electromagnetic solver loaded the temperature distribution determined by the thermal solver in the initial simulation and repeated the electromagnetic simulation. As a result, an updated power loss distribution was determined. The data were again transferred to the thermal solver, performing another 100 iterations. This procedure was repeated until the convergence was achieved. Usually, four repetitions of two-way coupled simulations were needed to converge. In the last step, 1000 iterations were further performed in the thermal solver to achieve reliable convergence in residuals, temperature distribution and mass flow rates through the most critical interfaces.

3.7. Boundary conditions and material properties

Two mutually distinct setups were used for the electromagnetic and thermal solvers. As explained in Section 3.4, the electromagnetic solver required only components under high potential. The current was introduced in cable connections using a boundary condition for the eddy-current solver. A neutral point connected all three phases at the other end of the current path; no boundary condition was associated. The complete current path was enclosed in a computational domain, allowing eddy currents to be propagated. As for materials and their properties, only aluminium and copper were used, with material properties defined in an electromagnetic solver library. Since the bulk conductivity heavily depends on the temperature, its thermal modifier was adopted.

The setup for the thermal solver was more complex than that for the electromagnetic solver. Around the entire switchgear, a sufficiently extensive computational domain was created to capture phenomena outside the switchgear. The domain had two major parts. One part was a cylindrical domain around the switchgear, with a radius of the cylinder larger than twice the height of the switchgear. Another part, positioned at the top of the cylindrical domain, was a bullet-shaped head to mitigate numerical diffusion and instabilities due to protruding from the sharp edges of the geometry. A no-slip wall boundary condition was used at the bottom surface of the cylindrical domain. The boundary conditions on the curvilinear surface of the cylinder and the bullet-shaped head were set up to a pressure outlet with the ambient temperature used as a backflow temperature.

The air domain inside the switchgear and its compartments comprised a combination of fluid domains, separated by 2D walls with

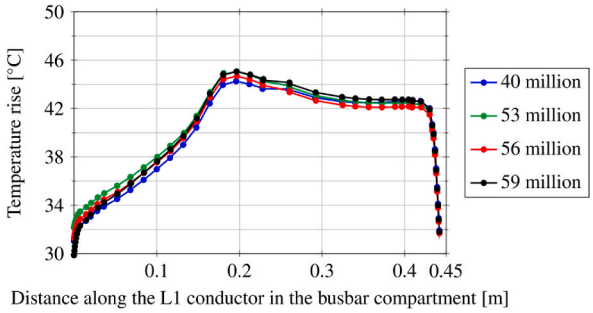

Fig. 5. Influence of the number of mesh elements on the temperature rise along a path above the L1 conductor in the busbar compartment.

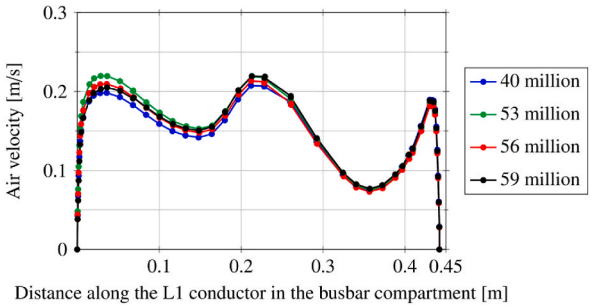

Fig. 6. Influence of the number of mesh elements on the air velocity along a path above the L1 conductor in the busbar compartment.

zero thickness and no-slip condition. Air could flow between these domains through their joint interfaces with a pressure drop condition representing sheet metal grids in the switchgear. Solid parts inside the switchgear were complex solid bodies. Some parts of solid bodies of the current path contained 2D zones with zero thickness to represent thin electrical insulation sleeves. The circuit breaker poles contained six heat pipes in pairs for each pole. Heat transfer related to heat pipes was modelled via a user-defined function (UDF). Based on the condenser and evaporator temperatures, the UDF determined heat fluxes used as boundary conditions.

As for material properties, material databases included in the simulation solvers were used. In the case of radiative heat transfer, the emissivity was a key parameter. The emissivity of most surfaces involved in the switchgear was experimentally measured in a lab at Brno University of Technology using a prototype of the switchgear. Such experimental data then served as inputs to the computer simulations. For instance, in the case of the surface of copper conductors, the emissivity of 0.05 was used. This value was very close to the experimental results of Hus et al. [40], who reported an emissivity of 0.07.

4. Validation

The validation of the simulation model was twofold, including the comparison of temperatures and air velocities. Other authors also adopted a similar procedure, e.g. Bedkowski et al. [34], who used their validated model for follow-up simulation analyses [6,16,19]. Details of the experimental setup and the accuracy of temperature measurements in the TRT were described in Section 2, and therefore, they are not repeated here. As for the measurement of air velocity inside the switchgear, a hot-film anemometry probe and sensor EE75 produced by E + E Elektronik, Austria, was utilised [47]. The probe was a thin-film sensing element with an external cover for protection and with a flow direction control. The probe was connected to the sensor with an embedded display, and the measured data were gathered by a computer connected to the sensor. The EE75 assembly was equipped with an integrated temperature compensation, making it suitable for measuring air velocity up to 40 m/s in the temperature range from −40 °C to 120 °C. The accuracy depends on the range of measured air velocities. In this study, all measured air velocities ranged from 0.06 m/s to 2 m/s, for which the accuracy of the EE75 assembly declared by its manufacturer is ±0.03 m/s. Besides the measurement of air velocity, the EE75 assembly also allows the air temperature measurement in the range from −40 °C to 120 °C with an accuracy of ±0.5 °C.

The validation of the computer model for the switchgear was addressed through a comparison between the simulation and experimental data. A root mean squared error (RMSE), a commonly used measure for quantifying differences between two datasets, was used for qualitative assessment. The RMSE was evaluated for the quantities used in the validation, including the temperatures and

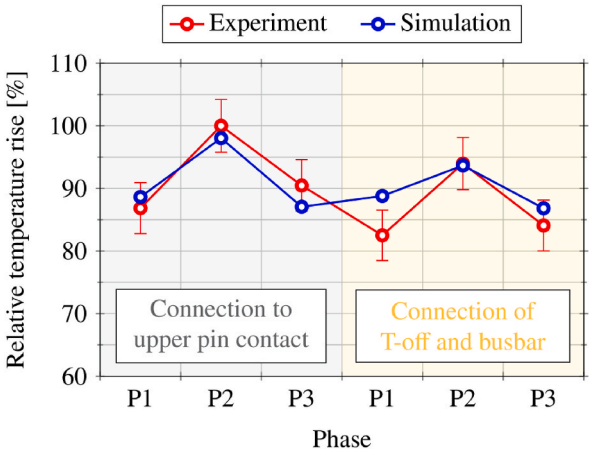

Fig. 7. Relative temperature rise for connections to upper pin contacts and connections of T-offs and busbars: Comparison between simulations and experiments for Design 2.

air velocities. The RMSE was determined as

$$\mathrm{RMSE}(y) = \sqrt{\frac{1}{n}\sum_{i=1}^{n}(\widetilde{y}_i - \widehat{y}_i)^2} \tag{9}$$

where $\widetilde{y}_i$ is a simulated value of a quantity y, $\widehat{y}_i$ is a corresponding experimental value, and n is the number of pairs (samples) of $\widetilde{y}_i$ and $\widehat{y}_i$.

4.1. Temperatures

As detailed in Section 5.1, five design modifications of the investigated medium-voltage switchgear were studied over the years, referred to as Design 1 to Design 5. A simulation model was developed for each of them, resulting in five models. Moreover, Design 3 was shape-optimised, resulting in (sixth) Design 3/O. Instead of the (absolute) temperature rise in degrees Celsius, results throughout this study are, due to confidentiality reasons, presented as the relative temperature rise in percentage with 100 % for the maximum value.

Fig. 7 compares the experimental and simulation results for Design 2 in terms of the relative temperature rise in the busbar compartment. Design 2 is, as discussed in Section 5, the most advanced improvement of the current state-of-the-art design. A comparison of experimental and simulation data for other designs, including Design 3 and Design 3/O, is presented in Section 5.4. The relative temperature rise in Fig. 7 is visualised for the connection to the upper pin contact of each phase (light grey background) and the connection of the T-off and busbar of each phase (light yellow background). Experimental data were acquired during the TRT, and the whiskers in Fig. 7 indicate the certified accuracy of the laboratory for temperature measurements (±1 % of the measured thermodynamic temperature). As can be seen in Fig. 7, good agreement between the simulation and experiment was achieved.

The RMSEs were evaluated using Eq. (9) and are listed in Table 2 to assess the simulation and experimental data. The RMSEs were determined only for Design 2, Design 3, and Design 3/O, as these were thoroughly investigated in TRTs. The determination of the RMSE for each case involved about thirty pairs $(\widetilde{T}_i, \widehat{T}_i)$ of the simulation and experimental temperatures along the current path of the investigated switchgear. Besides the RMSE, Table 2 also includes a normalised (scaled) RMSE, which was determined as a ratio between the RMSE and the average of the experimental temperatures $\widehat{T}_i$, both expressed in degrees Celsius. Considering the certified accuracy of experimentally determined temperatures, it can be concluded from the data in Table 2 that the simulation models of the switchgear can be regarded as good approximators of the experimentally determined temperatures along the current path.

Fig. 8, containing the data for Design 3/O, compares the simulated and experimental temperature rise at various other positions in switchgear compartments. The experimental measurement was repeated twice, referred to as Experiment 1 (red curve) and Experiment 2 (green curve). The EE75 assembly was utilised for the temperature rise measurements, with simultaneous measurement of the air velocity. As can be seen in Fig. 8, good agreement between simulation and experiments was obtained. Similarly, as in the case of the temperature rise in the busbar compartment, the average RMSE (considering the two sets of experimental data) for the temperatures presented in Fig. 8 was determined as 5.3 °C. The only position with a significant difference of more than 10 °C is the upper part of the air duct (position B in Fig. 8). A probable reason for such a discrepancy is a simplification in the air duct modelling. The duct was modelled using 2D elements with a defined thickness, which allowed consideration of heat transfer only in the perpendicular direction to these elements (surfaces). However, heat fluxes alongside the surfaces were not captured with this technique. This simplification probably led to underestimating the amount of heat accumulated by the duct, which could increase the temperature of the air flowing through the duct.

4.2. Air velocity

Fig. 9 compares the simulated and experimental air velocity at various other positions in switchgear compartments. Similarly, as in Fig. 8, the data in Fig. 9 are relevant for Design 3/O. The data were acquired during the experimental measurement, which was repeated twice using the EE75 assembly (air velocities and temperatures were measured concurrently). As can be seen, a good agreement between simulation results and experimental data was achieved. The average RMSE for the air velocities shown in Fig. 9 was determined to be 0.1 m/s. In contrast to the air temperatures (Fig. 8 and position B), no significant discrepancy was observed in any investigated positions.

Table 2
Validation and assessment of simulations and experiments in terms of RMSEs and normalised RMSEs of temperatures.

Dataset	RMSE [°C]	Normalised RMSE [%]
Design 2	2.29	3.2
Design 3	2.98	4.5
Design 3/O	3.03	4.8
Average	2.77	4.1

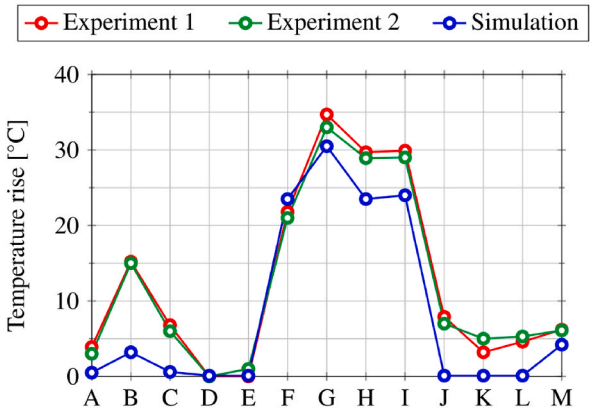

Fig. 8. Temperature rise for Design 3/O in various positions of the switchgear: Comparison between simulation and experiments. Positions: A - the inlet to the air duct; B - the outlet to the air duct; C - under the circuit breaker arm; D - directly in front of the partition plate; E – 50 mm in front of the partition plate; F - above the circuit breaker opening; G - above the busbar opening; H - above the cable compartment opening; I - air duct outflow; J - in front of the cable compartment flap; K - in front of the duct flap (upper opening); L - in from of the duct flap (lower opening); M – circuit breaker (under the lower heatsink).

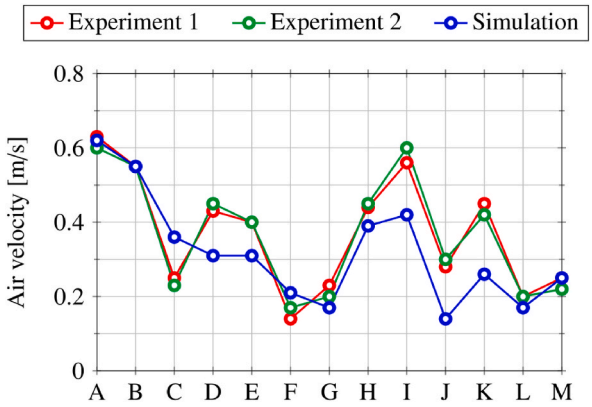

Fig. 9. Air velocity for Design 3/O in various positions of the switchgear: Comparison between simulation and experiments. Positions: identical to Fig. 8 (see its label).

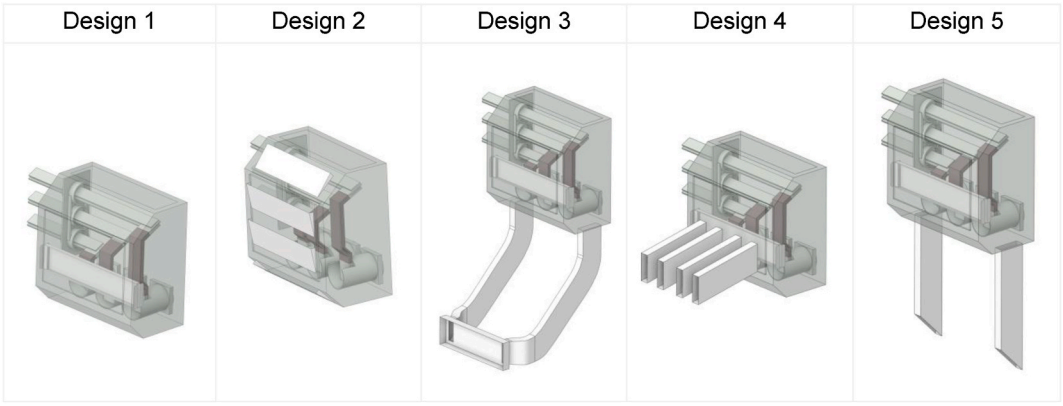

Fig. 10. Initial designs of busbar compartment cooling.

5. Results

The section with results is divided into three parts. First, air ducts were considered, and several (initial) designs for busbar compartment cooling were proposed. All designs were thoroughly investigated and compared to each other using computer simulations. Then, an experimental investigation, including the TRT, was carried out using a selected design. The experimental data for such a design demonstrated promising results; therefore, a design optimisation procedure was performed to improve the performance of the initial design further. Once completed, the optimised design was again investigated experimentally to confirm the results obtained in computer simulations.

5.1. Design of busbar compartment cooling

In the initial stage of the investigation, five designs (solutions) for busbar compartment cooling were proposed (referred to as Design 1 to Design 5) and are shown in Fig. 10. Design 1 was simple, including an enclosed busbar compartment except for its upper part with an opening. Such a design is currently widespread in the industry. Design 2 was an extension of Design 1 since it involved six wedge-shaped flaps integrated into the walls of the busbar compartment. Design 2 is the most advanced improvement of the current state-of-the-art design. Design 3 originated from Design 1, but it involved a two-channel air duct, which began in the cable compartment. The ambient air for cooling entered the two duct channels through a flap and flowed through the channels without further mixing with the air in the cable compartment.

Design 4 was based on the same idea as Design 3, involving four short horizontal ducts entering the busbar compartment from its vertical wall. Initially, only two horizontal ducts were considered, but preliminary results indicated their insufficient performance compared to Design 3. Due to this, the number of ducts gradually increased to four, which was a reasonable maximum from the viewpoint of internal arc risk. Design 5 was similar to Design 3 and Design 4, using air ducts. However, Design 5 involved two vertical air ducts, which collected the air from the bottom of the cable compartment, where the air temperature was relatively low compared to other positions of the cable compartment. The advantage of such a design is that no additional flaps were needed, which mitigated potential risks and costs.

5.2. Results of simulations under TRT conditions

In the initial step, the cooling performance and thermal behaviour of all the busbar compartment cooling designs were investigated through full-scale simulations of the complete switchgear. The computer models were configured to replicate actual conditions of the TRT, during which the switchgear is experimentally tested in practice. This configuration mainly included the switchgear loaded by an alternating three-phase current of 4000 A and a frequency of 50 Hz. The ambient air temperature was set to 31.4 °C in all simulations, corresponding to an average air temperature during the experimental TRTs. Further details and conditions under which the TRT was performed were described in Section 2. As discussed in Section 3, the computer simulations addressed coupled electromagnetics with conjugate heat transfer, including natural convection.

The computer simulations were solved as steady-state problems, assuming that the behaviour, characteristic parameters, and other quantities were stable in time. This assumption was confirmed in four cases: Design 2, Design 3, Design 4, and Design 5. In the case of Design 1, however, the simulation was solved as a transient problem since the key quantities, including the mass flow rate through the busbar compartment and the air temperature at the opening of the busbar compartment, fluctuated rather significantly, as discussed below.

In the case of Design 1, there was only a single opening at the upper horizontal surface of the busbar compartment. It means that the opening functioned periodically as an inlet as well as an outlet for the air, which was sucked into the busbar compartment, heated up, and left the busbar compartment due to natural convection. Fig. 11 shows the mass flow rate of air and its average temperature rise at the opening, which were determined in the transient simulation. The temperature rise refers to the difference between the actual and

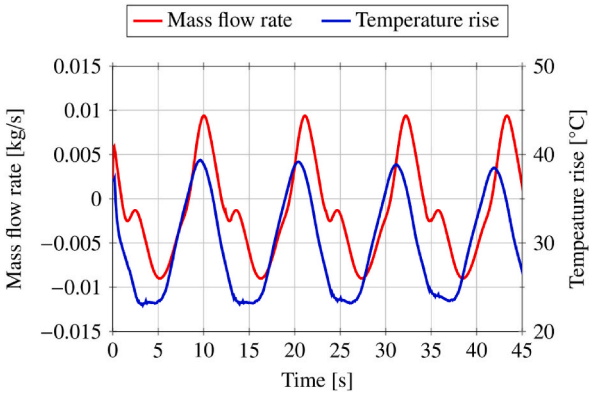

Fig. 11. Transient mass flow rate of air and its temperature at the opening of the busbar compartment for Design 1.

ambient air temperatures outside the switchgear. As can be seen, the mass flow rate of air and its average temperature at the opening fluctuated in time with a period of about 11 s. Such behaviour indicated that the opening served as an inlet for a specific part of the period and an outlet for the rest. The temperature rise varied significantly from about 23 °C to almost 40 °C. As for the mass flow rate, its mean value was zero, with fluctuations having a magnitude of about 0.01 kg/s.

Design 2 was an extension of Design 1 as it incorporated six wedge-shaped flaps integrated into the walls of the busbar compartment. As indicated in Fig. 10, four flaps were located on vertical and inclined (front) surfaces facing the cable compartment. The other two flaps were on the opposite (rear) vertical surface facing the circuit breaker compartment. The simulations revealed that the four flaps on the front surface of the busbar compartment served, on average, as inlets, while two flaps on the rear surface served (on average) as outlets. The mass flow rate of air entering the busbar compartment through these inlet flaps was 0.2699 kg/s, with the average temperature rise at the inlets of 40.30 °C.

Designs 3 to 5 incorporated ducts for feeding the air into the busbar compartment; therefore, they could be directly compared. Table 3 summarises the simulation results for these designs, including the mass flow rate through the duct systems to the busbar compartment and the average temperature rises at the inlet and outlet of the duct system. As can be seen, Design 4 led to the highest mass flow rate of air, followed by Design 3 and Design 5. The temperature of air entering the busbar compartment was quite similar, ranging from about 3 °C to about 5 °C.

Further, the relative temperature rise at nine positions in the busbar compartment was determined to assess the heat withdrawal capability of the proposed designs. These positions included tree spots along the current path of each phase, including the connection to the upper pin contact (positions 1–3 in Fig. 1), the connection of the T-off with the busbar (positions 4–6 in Fig. 1), and the end of the busbar (positions 7–9 in Fig. 1). Table 4 presents the complete results for all investigated designs. The most critical positions with the highest relative temperature rise were associated with (middle) phase L2: the connection to the upper pin contact and the connection of the T-off with the busbar. The reason is quite apparent: phase L2 is surrounded by the (peripheral) phase L1 and phase L3 from both its sides, contributing to the thermal load. Further, the additional load is also caused by the proximity effect, redistributing the current in parallel conductors.

As seen from Table 4, for Designs 2, 3, and 4, the highest relative temperature rise was observed in the connection to the upper pin contact for phase L2. On the contrary, for Design 1 and Design 5, the highest relative temperature rise was in the connection of the T-off with the busbar for phase L2. Further, the data analysis in Table 4 revealed that the lowest maximum relative temperature rise was achieved in Design 3. Indeed, the maximum relative temperature rise was 25 % lower than in the case of Design 1, which is a standard design used in the industry. The maximum relative temperature rise for Design 4, Design 5, and Design 2 was about 4 %, 7 %, and 12 % higher than for Design 3, respectively, and in all cases significantly lower than Design 1. It is also worth mentioning that even though Design 4 outperformed Design 3 in terms of the mass flow rate of air flowing through the duct to the busbar compartment as well as in terms of the temperature rise at the duct outlet (Table 3), lower values of the temperature rise (Table 4) were finally achieved with Design 3 than with Design 4. It makes Design 3 the best solution among others in terms of the cooling performance of the busbar compartment. Based on these results, Design 3 was selected as a baseline solution for design optimisation, which could further improve its thermal (cooling) performance. This procedure is presented in detail in the following Section 5.3.

5.3. Design optimisation of the duct

The Adjoint Solver module for ANSYS Fluent was utilised for shape optimisation of Design 3, which served as a baseline (initial) solution. The optimisation was aimed at reducing the pressure drop of the duct system as it would increase the mass flow rate of air supplied to the busbar compartment. Fig. 12 compares the baseline Design 3 and its shape-optimised version, referred to as Design 3/O, in terms of the velocity field visualised by the line integral convolution. As shown in Fig. 12(a), the baseline design suffered from boundary layer separations, primarily due to sharp edges in the duct design. As a result, the boundary flow separation led to an increased pressure loss of the duct, limiting its ability to supply the air (in terms of its mass flow rate) to the busbar compartment. Shape optimisation of the duct system led to a modification of the baseline design, resulting in the removal of the sharp edges and a slight modification of the geometry of the duct inlet, as shown in Fig. 12(b). The analysis of data in Fig. 12 (the comparison of baseline and optimised designs) indicates that no flow separations are associated with the shape-optimised Design 3/O (Fig. 12(b)).

Table 5 summarises the comparison of the baseline Design 3 and its shape-optimised Design 3/O in terms of the mass flow rate of air flowing through the duct, its total pressure, and the air temperature rise at the inlet and outlet. As indicated in Table 5, removing the sharp edges with aerodynamic optimisation and improving the duct geometry allowed for about a 57 % reduction in the total pressure loss of the duct system. As a result, the mass flow rate of air in the optimised duct system increased by about 12 % compared to the baseline design. On the other hand, air temperature rise along the ducts remained virtually unchanged, as the temperature changes presented in Table 5 are minimal. Overall, the shape-optimised Design 3/O brought significant improvements compared to the baseline Design 3. A comprehensive analysis is presented in Section 5.4 to address the performance of the optimised Design 3/O.

Table 3
Results of computer simulations under TRT conditions for designs with a duct system.

Quantity	Design 3	Design 4	Design 5
Mass flow rate through duct [kg/s]	0.0156	0.0199	0.0102
Temperature rise at duct inlet [°C]	0.36	0.51	2.93
Temperature rise at duct outlet [°C]	4.07	2.89	4.81

Table 4
Comparison of the relative temperature rise along the current path in the busbar compartment.

Solution	Phase	Relative temperature rise [%]			
		Connection to the upper pin contact	Connection of T-off with busbar	End of busbars	Average over all phases
Design 1	L1	93.3	97.6	67.1	86.8
	L2	95.6	**100.0**	69.9	
	L3	94.8	96.8	66.0	
Design 2	L1	78.4	78.6	56.9	72.5
	L2	**86.8**	82.9	57.8	
	L3	77.0	76.8	57.3	
Design 3	L1	74.7	69.1	56.6	66.8
	L2	**75.0**	71.6	57.5	
	L3	73.2	66.3	56.5	
Design 4	L1	76.4	74.8	58.4	70.3
	L2	**79.1**	78.2	57.8	
	L3	77.7	73.2	57.3	
Design 5	L1	78.2	79.6	56.6	72.6
	L2	80.3	**81.9**	59.0	
	L3	79.6	80.3	58.7	

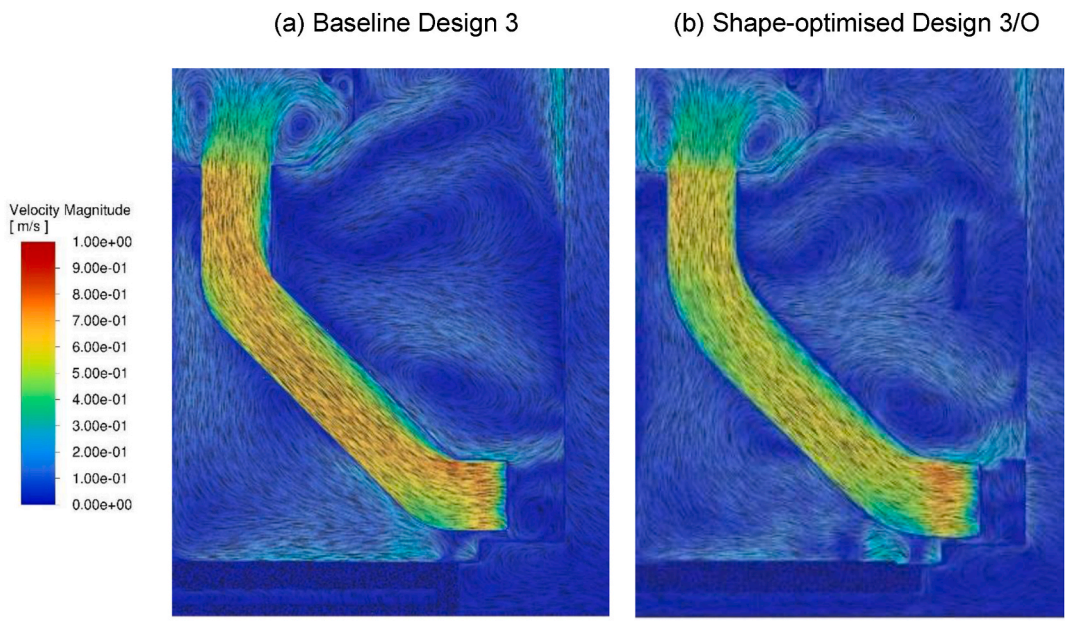

Fig. 12. Velocity field visualised with the line integral convolution for the baseline Design 3 and its shape-optimised Design 3/O.

Table 5
Comparison of baseline Design 3 and its shape-optimised Design 3/O.

Solution	Mass flow rate [g/s]	Pressure loss [mPa]	Temperature rise [°C]	
			Duct inlet	Duct outlet
Design 3 (baseline)	15.6	385	0.36	0.35
Design 3/O (optimised)	17.6	163	4.07	3.79

Further, the thickness of the duct walls and their influence on the cooling capability of air in the busbar compartment were investigated. This viewpoint was motivated by the fact that a thermally insulated duct preventing air from being heated from the cable compartment could feed colder air to the busbar compartment for cooling. Fig. 13 presents the relative temperature rise in the busbar compartment in dependence on the thickness of the duct walls for the middle phase L2. The material of the duct walls was plastic. As explained in Section 4.1, the duct walls were modelled using a simplified approach, including 2D elements with a defined virtual thickness. The data in Fig. 13 indicate that the increase in the wall thickness (i.e. the increase in the thermal resistance of the wall) led to the decrease in the relative temperature rise along the current path in the busbar compartment. However, the drop in the relative temperature rise was relatively small when the wall thickness (thermal resistance) increased. For example, the thickness of the duct

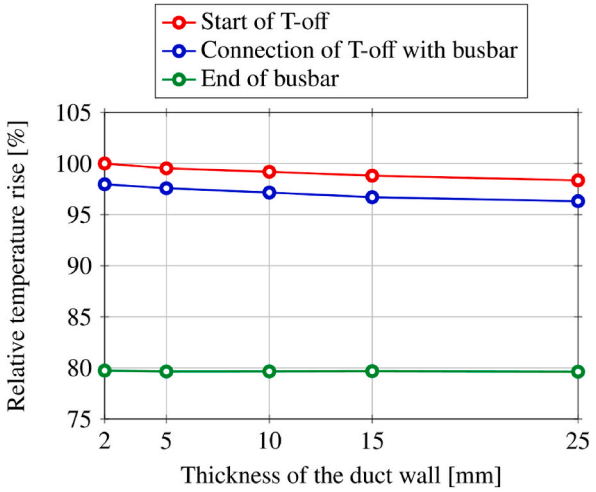

Fig. 13. Influence of the thickness of the duct walls on the relative temperature rise of the current path (phase L2) in the busbar compartment.

walls of 25 mm, equivalent to the thermal insulation layer with a thermal resistance of about 0.12 (m^2K)/W, would cause the average drop in the temperature rise of only about 1 %. As a result, the thermal insulation of the duct does not represent a measure with a potential for significant improvement in the busbar compartment cooling.

5.4. Thermal analysis of busbar compartment with shape-optimised design

The influence of the shape-optimised Design 3/O on the busbar compartment was further analysed in detail using computer simulations, addressing other viewpoints such as the relative temperature rise in individual conductors of the busbar, the power loss distribution in conductors of the busbars, and the air velocity distribution in the vicinity of the busbars. In this analysis, Design 3/O was compared to Design 2 (Fig. 10). Design 2 was an extended version of simple Design 1, which used flaps to enhance cooling performance. Design 2 is currently the most advanced improvement of the current state-of-the-art design, and it is used where higher requirements on the current rating of the switchgear are required compared to Design 1.

Fig. 14 shows the relative temperature rise in the individual conductors (referred to as conductor A, conductor B, and conductor C) of the busbar for the middle phase L2, as this busbar was the most critical one among others in terms of the relative temperature rise, as explained in the foregoing sections. The data in Fig. 12 indicate that Design 3/O, compared to Design 2, allowed a reduction in the relative temperature rise of about 15 % in the connection of the busbar with the T-off (position 5 in Fig. 1). The reduction (difference) in the relative temperature rise gradually decreased along the busbar when the distance from the connection of the busbar with the T-off increased. At the end of the busbar (position 8 in Fig. 1), the difference in the relative temperature rise between Design 3/O and Design 2 was almost negligible (around 1 %). It is also worth pointing out that the relative temperature rise of individual conductors was different for individual conductors but identical in the connection of the busbar with the T-off and at the end of the busbar, since the conductors were in thermal contact due to joints in these spots. An interesting observation is that the relative temperature rise was almost linear for the outer conductors A and C, which are only marginally influenced by the proximity effect. On the other hand, the relative temperature rise for conductor B was strongly non-linear and influenced by the proximity effect as the outer conductors A and C surrounded conductor B from two sides.

Fig. 15 shows the comparison of air velocity and its distribution in the busbar compartment for Design 2 (Fig. 15(a)) and Design 3/O (Fig. 15(b)). The data demonstrate that in comparison of Design 2 with Design 3/O, the air velocity in the busbar compartment was very different. The higher and more evenly distributed air velocity was in Design 2. On the other hand, in Design 3/O with the shape-optimised duct, there was a substantial air inflow to the busbar compartment from the duct, directly flowing along the busbars, though with some air flow recirculation on the sides of the inlet. In both designs, higher airflow velocities were in the vicinity of the busbars rather than in the remaining space of the busbar compartment. However, when the magnitude of the air velocity is considered, higher values were achieved with Design 2 than with Design 3/O.

The data presented throughout Section 5 clearly demonstrate that the utilisation of ducts was beneficial. The initial hypothesis was that the ducts could reduce the temperature rise of the air entering the busbar compartment. Further, it was also anticipated that the heat transfer coefficient could reach greater values due to the mitigation of the transient behaviour (fluctuations) at the busbar openings (shown in Fig. 11) and due to the intensified chimney effect coupled with the intensified air flow through the busbar compartment. However, the evaluation of the heat transfer coefficient on the surfaces of the conductors showed that the value of the heat transfer coefficient was virtually constant in all cases. Regardless of the use of ducts or their modification, the value of the heat transfer coefficient was about 4 W/(m^2K), which agrees with the findings reported by Zheng et al. [22]. A probable explanation for this behaviour can be observed in Fig. 15. The duct fed the air to the busbar compartment, but due to its complex shape, the air flow structure rapidly disintegrated after leaving the duct and separated into a number of vortices. As a result, no uniform air flow structure

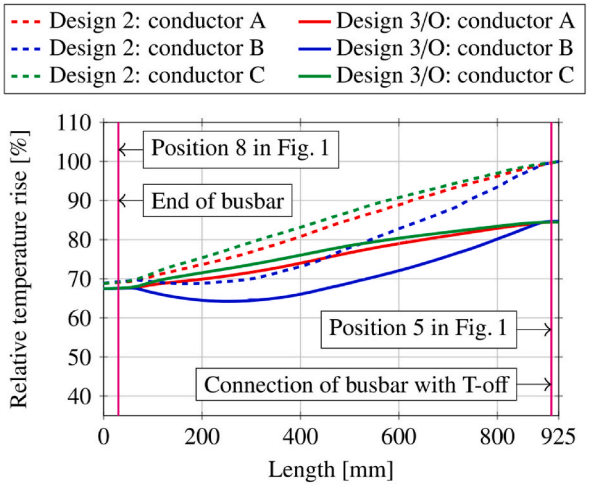

Fig. 14. Relative temperature rise in conductors of the busbar: Comparison of Design 3/O with Design 2.

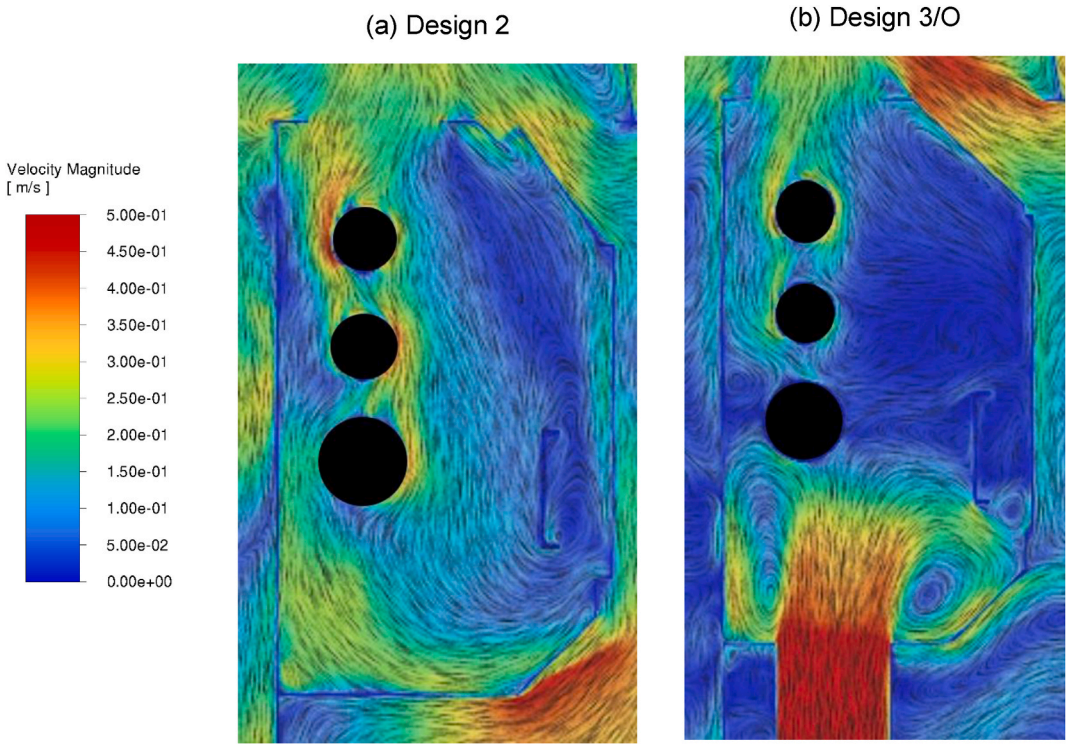

Fig. 15. Comparison of air velocity in the busbar compartment for (a) Design 2 and (3) Design 3/O. The cross-sections of the busbars with their conductors are intentionally filled in black due to confidentiality reasons.

was achieved in the busbar compartment. Therefore, the key factor related to the use of ducts was a reduced temperature of air entering the busbar compartment. No significant improvement was associated with an additional thermal insulation of the ducts, as demonstrated in Fig. 13. On the other hand, the shape optimisation of the duct geometry further increased the air mass flow rate due to reduced pressure losses, contributing to the reduction of the air temperature entering the busbar compartment.

5.5. Experimental investigation of shape-optimised design

Besides the computer simulations, the influence of the shape-optimised Design 3/O on thermal conditions in the busbar compartment was also investigated experimentally. Results were compared with the baseline (unoptimised) Design 3 and the flap-

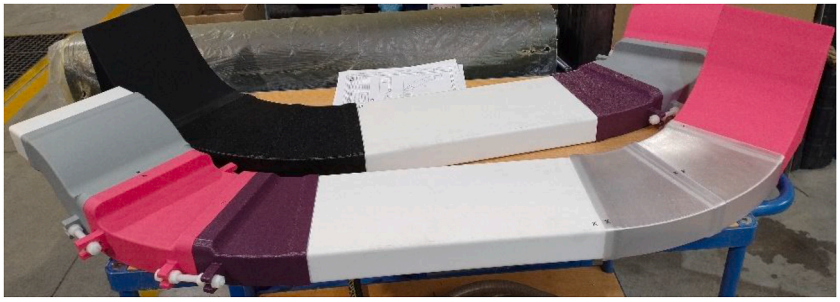

Fig. 16. 3D-printed prototype of the ducts for Design 3/O and its experimental investigation.

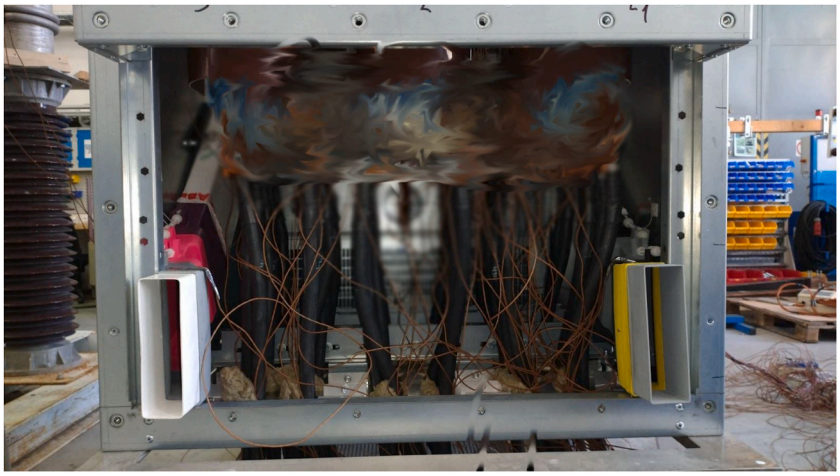

Fig. 17. Preparation of the switchgear for the TRT with visible duct intakes of Design 3/O and wiring (yet not settled) of thermocouples in the cable compartment. The cable connection is intentionally blurred due to confidentiality reasons.

based Design 2. Fig. 16 shows a photograph of a 3D-printed prototype of the duct system of Design 3/O, which was used in the experimental investigation. 3D printing was the only reasonable technology for manufacturing the duct prototype due to its complex (curved) shape. The prototype was made of PLA and PETG plastic materials and consisted of several parts due to the limitations of the 3D printer. The parts were then assembled into the complete ducts using bolt connections. Fig. 17 is a photograph showing the installation of the 3D-printed ducts of Design 3/O into the busbar compartment of the switchgear and its preparation for the TRT. The

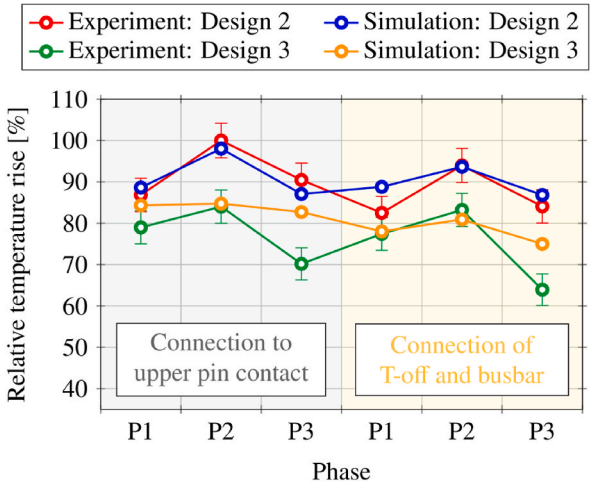

Fig. 18. Relative temperature rise for the busbar compartment: Comparison of simulation and experimental data between Design 2 and Design 3.

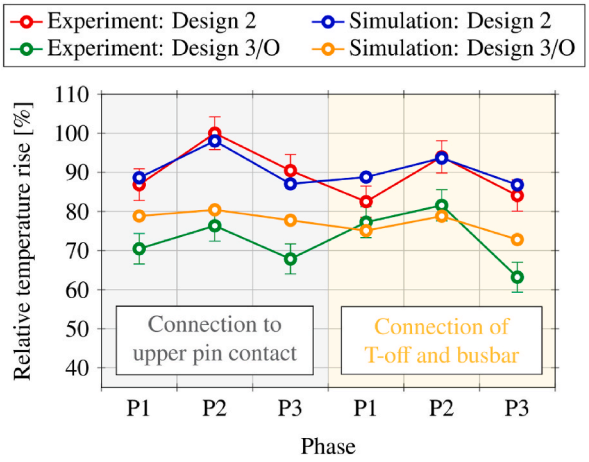

Fig. 19. Relative temperature rise for the busbar compartment: Comparison of simulation and experimental data between Design 2 and Design 3/O.

intakes to the ducts are visible in Fig. 17, as a front cover made of sheet metal was removed during the installation.

Fig. 18 compares the relative temperature rise in the busbar compartment between Design 2 and Design 3, including simulation data and experimental data from the TRTs. As can be seen, the relative temperature rise for Design 3 was about 10 %–15 % lower than that of Design 2. Fig. 19 shows an identical comparison between Design 2 and shape-optimised Design 3/O. The conclusion is similar to that of Fig. 18, but the reduction of the relative temperature rise was higher. The relative temperature rise for Design 3/O was approximately 15 %–20 % lower when compared to Design 2. Moreover, the comparison of data in Figs. 18 and 19 for Design 3 and Design 3/O indicates that the shape-optimisation of the duct system indeed improved the thermal conditions (cooling) in the busbar compartment, as the relative temperature rise for Design 3/O was about 5 % lower when compared to Design 3.

6. Conclusion

The study reported on a detailed investigation of the thermal management of an air-insulated medium-voltage electrical switchgear, which is commonly used in practice as a part of the electrical grid. Full-scale two-way coupled multiphysical simulations and standardised temperature rise tests were performed. Several designs for enhanced cooling were proposed and studied to increase the current rating of the switchgear with no additional expenses. An innovative design for enhanced cooling in the busbar compartment using ventilation ducts, which was proposed by the lead author and thoroughly investigated in the present study, was recently patented [48]. The main conclusions.

- A design of the busbar compartment of the switchgear with a single opening on its top, a standard design used in industrial switchgear, led to the worst results among other studied designs. An improved design of the busbar compartment, including ventilation flaps for improved cooling and higher current ratings, indicated better performance. In spite of this, it was still considered unsatisfactory.
- Three other designs, which included ventilation ducts feeding the air into the busbar compartment, showed superior performance compared to designs of the busbar compartment with a single opening on its top and with ventilation flaps. The maximum relative temperature rise in the busbar compartment for the three designs with ventilation ducts was about 5 %–20 % lower than in the designs without the ducts.
- The best-performing design of the busbar compartment with a two-channel air duct led to a lower relative temperature rise by about 5 %–20 % compared to the designs without the ducts. In the next step, the design (shape) of the two-channel air duct was further shape-optimised for reducing pressure drop, allowing an increase in air mass flow rate for enhanced cooling.
- The shape optimisation of the two-channel air duct system led to a 57 % reduction in its pressure drop. As a result, the air mass flow rate necessary for enhanced cooling of the busbar compartment increased by approximately 12 %.
- The shape-optimised two-channel ventilation duct allowed for a lower relative temperature rise in the busbar compartment by about 15 %–20 % compared to the design with ventilation flaps, which is currently the most advanced improvement of the state-of-the-art design used in industrial switchgears.

In the next step, further design optimisation of the duct geometry, together with the determination of the cutoff current rating and a detailed economic assessment, will be needed for the implementation of the proposed modifications into commercially produced switchgears.

CRediT authorship contribution statement

Ondřej Novák: Writing – original draft, Visualization, Validation, Software, Methodology, Investigation, Formal analysis, Data curation, Conceptualization. **Lubomír Klimeš:** Writing – review & editing, Visualization, Supervision, Project administration, Methodology, Funding acquisition, Formal analysis.

Declaration of competing interest

The authors declare the following financial interests/personal relationships which may be considered as potential competing interests: Lubomir Klimes reports financial support was provided by Czech Science Foundation. Ondrej Novak reports financial support was provided by Technology Agency of the Czech Republic. Lubomir Klimes reports financial support was provided by European Union through the Ministry of Education, Youth and Sports of the Czech Republic. Ondrej Novak reports financial support was provided by ABB. Ondrej Novak has patent Low or medium voltage switchgear, EP4459816A1, 2024 pending to European Patent Office. If there are other authors, they declare that they have no known competing financial interests or personal relationships that could have appeared to influence the work reported in this paper.

Acknowledgement

The work was supported by the Technology Agency of the Czech Republic (project reg. no. TK04020256), by ABB Ltd., by the project The Energy Conversion and Storage, funded as project reg. no. CZ.02.01.01/00/22_008/0004617 by Programme Johannes Amos Comenius, call Excellent Research, and by the project Machine learning-based surrogate modeling for conjugate heat transfer enhancement with complex surface geometry, funded as project reg. no. 25-16935S by the Czech Science Foundation.

Nomenclature

Latin letters

B	magnetic field
c_p	heat capacity at constant pressure
E	electric field
g	gravitational acceleration
J	current density
k	thermal conductivity
n	number of samples in a set
p	pressure
$\dot{Q}_s$	internal volumetric heat source
t	time
T	temperature
u	velocity
y	general quantity
$\widehat{y}$	simulated value of quantity y
$\widetilde{y}$	measured value of quantity y

Greek letters

ε_0	vacuum permittivity
μ	dynamic viscosity
μ_0	vacuum permeability
ϱ	density of the matter
ϱ_0	reference density of the matter
ϱ_e	density of electrical charge
σ	electrical conductivity

Abbreviations

ADI	alternating direction implicit
CFD	computational fluid dynamics
DO	discrete ordinate
EMAG	electromagnetic
FEM	finite element method
HVAC	heating, ventilation, and air conditioning
IEC	International Electrotechnical Commission
PCM	phase change material

PDE	partial differential equation
PFAS	per- and polyfluoroalkyl substances
RANS	Reynolds-averaged Navier-Stokes
RMSE	root mean squared error
RNG	renormalisation group
SST	shear stress transport
TRT	temperature rise test
UDF	user-defined function

Data availability

The authors do not have permission to share data.

References

[1] Air Insulated Switchgear Market Report 2020-2030. Visiongain; n.d.
[2] International Electrotechnical Commission (IEC), IEC 62271-200 high-voltage Switchgear and Controlgear - Part 200: AC metal-enclosed Switchgear and Controlgear for Rated Voltages Above 1 Kv and up to and Including 52 Kv, IEC, 2021.
[3] M Runde, Failure frequencies for high-voltage circuit breakers, disconnectors, earthing switches, instrument transformers, and gas-insulated switchgear, IEEE Trans. Power Deliv. 28 (2013) 529–530.
[4] X Zhou, J Yi, R Song, X Yang, Y Li, H Tang, An overview of power transmission systems in China, Energy (Oxf) 35 (2010) 4302–4312.
[5] Handbook of Switchgears, McGraw Hill Higher Education, Maidenhead, England, 2006.
[6] M Bedkowski, J Smolka, Z Bulinski, A Ryfa, 2.5-D multilayer optimisation of an industrial switchgear busbar system, Appl. Therm. Eng. 101 (2016) 147–155.
[7] M Stosur, M Szewczyk, K Sowa, P Dawidowski, P Balcerek, Thermal behaviour analyses of gas-insulated switchgear compartment using thermal network method, IET Gener. Transm. Distrib. 10 (2016) 2833–2841.
[8] SL Ho, Y Li, W Edward, C Lo, JY Xu, X Lin, Analyses of three-dimensional eddy current field and thermal problems in an isolated phase bus, IEEE Trans. Magn. 39 (2003) 1515–1518.
[9] W Anbo, C Degui, W Jianhua, C Bin, G Yingsan, Evaluation of thermal performance for air-insulated busbar trunking system by coupled magneto-fluid-thermal fields, in: Proceedings. International Conference on Power System Technology, IEEE, 2003, https://doi.org/10.1109/icpst.2002.1047164.
[10] J Wang, L Liu, E Wang, Study on numerical simulation of flow and temperature fields inside isolated phase bus based on fluent, in: 2007 International Conference on Electrical Machines and Systems (ICEMS), IEEE, 2007, https://doi.org/10.1109/icems12746.2007.4412079.
[11] J Paulke, H Weichert, P Steinhauser, Thermal simulation of switchgear, in: Proceedings of the Forth-Seventh IEEE Holm Conference on Electrical Contacts (IEEE Cat. No.01CH37192), IEEE, 2002, https://doi.org/10.1109/holm.2001.953183.
[12] SW Kim, HH Kim, SC Hahn, BY Lee, KY Park, YJ Shin, et al., Coupled finite-element-analytic technique for prediction of temperature rise in power apparatus, IEEE Trans. Magn. 38 (2002) 921–924.
[13] JK Kim, SC Hahn, KY Park, HK Kim, YH Oh, Temperature rise prediction of EHV GIS bus bar by coupled magnetothermal finite element method, IEEE Trans. Magn. 41 (2005) 1636–1639.
[14] X Guan, N Shu, H Peng, LBM simulation of heat transfer processes inside GIS capsule filled with different insulation gas mixtures, Math. Comput. Simulat. 188 (2021) 212–225.
[15] B Wang, X Jia, J Yang, Q Wang, Numerical study on temperature rise and structure optimization for a three-phase gas insulated switchgear busbar chamber, Energy (Oxf) 254 (2022) 124463.
[16] M Bedkowski, J Smolka, K Banasiak, Z Bulinski, AJ Nowak, T Tomanek, et al., Coupled numerical modelling of power loss generation in busbar system of low-voltage switchgear, Int. J. Therm. Sci. 82 (2014) 122–129.
[17] X Zheng, F Hu, Y Wang, H Zhang, S You, R Shi, et al., Optimization on airflow distribution for anti-condensation of high-voltage switchgear using CFD method, Case Stud. Therm. Eng. 28 (2021) 101479.
[18] S Shu, Z Zhan, J Xu, Y Huang, W Huang, Y Lin, Three-dimensional numerical simulation and experiment of moisture condensation mechanism inside high voltage switchgear, Int. J. Electr. Power Energy Syst. 151 (2023) 109129.
[19] M Bedkowski, J Smolka, Z Bulinski, A Ryfa, Simulation of cooling enhancement in industrial low-voltage switchgear using validated coupled CFD-EMAG model, Int. J. Therm. Sci. 111 (2017) 437–449.
[20] M Matin, A Dehghanian, AH Zeinaddini, H Darijani, Interpretable machine learning modeling of temperature rise in a medium voltage switchgear using multiphysics CFD analysis, Case Stud. Therm. Eng. 65 (2025) 105585.
[21] MA Aguirre, M Bierzychudek, DN Coppa, HM Laiz, Virtual experiment of temperature rise test in high-voltage switchgear, Measurement: Sensors 38 (2025) 101494.
[22] W Zheng, X Jia, Z Zhou, J Yang, Q Wang, Multi-physical field coupling simulation and thermal design of 10 kV-KYN28A high-current switchgear, Therm. Sci. Eng. Prog. 43 (2023) 101954.
[23] S Cheng, Y Zhao, K Xie, B Hu, J Zhang, X Yang, A novel method for fast computation of the temperature rise and optimal design of GIL based on thermal network model, Energy 289 (2024) 130034.
[24] P Qu, J Cheng, Y Chen, Y Li, W Li, H Tao, Numerical and experimental investigation on heat transfer of multi-heat sources mounted on a fined radiator within embedded heat pipes in an electronic cabinet, Int. J. Therm. Sci. 183 (2023) 107833.
[25] P MF Kaufmann, Cooling Apparatus for Switchgear with Enhanced Busbar Joint Cooling, 2014, 8717746B2.
[26] H Yu, P Yang, H Yao, H Li, Y Li, H Tao, Multi-physics coupling-based numerical simulation and optimization of heat pipe cooling systems for sealed switchgear, Int. J. Therm. Sci. 215 (2025) 109983.
[27] P Kaufmann, O Sologubenko, F Molitor, T Buehler, Switchgear Cooling System Comprising a Heat Pipe, Fan and Thermoelectric Generation, 2016, 2016/116410 A1.
[28] Fluorinated Gases and ozone-depleting Substances: Council and Parliament Reach Agreement, Council of the European Union, 2023. https://www.consilium.europa.eu/en/press/press-releases/2023/10/05/fluorinated-gases-and-ozone-depleting-substances-council-and-parliament-reach-agreement/. (Accessed 11 March 2025).
[29] M Kessler, A Stadnicki, O Sologubenko, O Fussbahn, O Claus, Cooling Apparatus for a Medium Voltage or High Voltage Switchgear, 3889985A1, 2021.
[30] M Kessler, O Sologubenko, J Hemrle, A Rybak, A Michalik, Cooling Apparatus for a Medium Voltage or High Voltage Switchgear, 2022, 2022/0074672A1.
[31] L David, Passive Cooling of the Busbar Compartment of the Electrical Switchgear, Brno University of Technology, 2025. MSc thesis.
[32] A Miaari, HM Ali, Recent advances on nano-enhanced phase change materials (NEPCMs) for photovoltaic thermal management and role of machine learning: a review of fundamentals, preparation, characterization, and thermo-physical properties, J. Energy Storage 124 (2025) 116544.

[33] A Kumar Thakur, R Sathyamurthy, R Velraj, R Saidur, AK Pandey, Z Ma, et al., A state-of-the art review on advancing battery thermal management systems for fast-charging, Appl. Therm. Eng. 226 (2023) 120303.
[34] M Bedkowski, J Smolka, Z Bulinski, A Ryfa, M Ligeza, Experimentally validated model of coupled thermal processes in a laboratory switchgear, IET Gener. Transm. Distrib. 10 (2016) 2699–2709.
[35] J Gastelurrutia, JC Ramos, GS Larraona, A Rivas, J Izagirre, L del Río, Numerical modelling of natural convection of oil inside distribution transformers, Appl. Therm. Eng. 31 (2011) 493–505.
[36] JK Sigey, FK Gatheri, M Kinyanjui, Numerical study of free convection turbulent heat transfer in an enclosure, Energy Convers. Manag. 45 (2004) 2571–2582.
[37] A Behzadmehr, N Galanis, A Laneville, Low Reynolds number mixed convection in vertical tubes with uniform wall heat flux, Int. J. Heat Mass Tran. 46 (2003) 4823–4833.
[38] AG Fedorov, R Viskanta, Turbulent natural convection heat transfer in an asymmetrically heated, vertical parallel-plate channel, Int. J. Heat Mass Tran. 40 (1997) 3849–3860.
[39] L Shao, SB Riffat, Accuracy of CFD for predicting pressure losses in HVAC duct fittings, Appl. Energy 51 (1995) 233–248.
[40] J Hus, Estimating busbar temperatures. Industrial applications society, in: 36th Annual Petroleum and Chemical Industry Conference, IEEE, 1989, https://doi.org/10.1109/pcicon.1989.77873.
[41] Temperature Rise Test Report, ABB Inc, 2023.
[42] D Anderson, JC Tannehill, RH Pletcher, R Munipalli, V Shankar, Computational Fluid Mechanics and Heat Transfer, CRC Press, 2020.
[43] JD Kraus, in: Electromagnetics, fifth ed., McGraw-Hill, New York, NY, 1998.
[44] DJ Griffiths, Introduction to Electrodynamics, Cambridge University Press, Cambridge, England, 2017.
[45] WH Hayt, Engineering Electromagnetics, McGraw-Hill, New York, NY, 2018.
[46] ANSYS Fluent 14 Software Documentation, ANSYS Inc, 2011.
[47] Datasheet EE75, Highly Accurate air/gas Velocity Sensor for Industrial Applications, E+E Elektronik, 2023.
[48] O Novák, Low or Medium Voltage Switchgear, 2024, 4459816A1.